11th International Symposium on Turbulence and Shear Flow Phenomena (TSFP11)
Southampton, UK, July 30 to August 2, 2019

CHARACTERIZING ENERGY TRANSFER IN RESTRICTED NONLINEAR WALL-BOUNDED TURBULENCE

Benjamin A. Minnick
Department of Mechanical Engineering
Johns Hopkins University
3400 N. Charles St. Baltimore, MD, 21218, USA
bminnic2@jhu.edu

Dennice F. Gayme
Department of Mechanical Engineering
Johns Hopkins University
3400 N. Charles St. Baltimore, MD, 21218, USA
dennice@jhu.edu

ABSTRACT

The restricted nonlinear (RNL) model predicts low-order statistics of wall-bounded turbulent flows at low to moderate Reynolds numbers. We demonstrate that the accuracy of this prediction depends on its streamwise wavenumber support, which is optimized when the associated modes coincide with the outer layer peak of the surrogate dissipation spectra. The structures associated with this peak range asymptote to a streamwise extent of 150 wall units making RNL a predictive reduced-order model for wall-bounded turbulence. We then expand upon the current understanding of the RNL system by comparing the energy transfer when the dynamics are supported by the low wavenumbers associated with unparameterized RNL dynamics to those associated with reproducing the correct log-law behavior. Our results show that the correct parametrization improves the predictions of spectra and energy transport. However, the RNL dynamics seem to compensate for the reduction in dissipation associated with the dynamic restriction on the nonlinear interactions by shifting the energy of the spanwise spectra peaks to smaller scales and increasing turbulent and viscous transport rates near the wall. These observations suggest that the self-sustaining process underlying the RNL dynamics is very robust, which may have implications for flow control strategies aimed at reducing turbulence.

INTRODUCTION

Numerical and experimental studies have shown evidence that coherent structures elongated in the streamwise direction play a crucial role in the dynamics of wall-bounded turbulent flow (see, e.g. Smits et al. 2011). Near the wall where majority of the energy is dissipated, streaky flow structures and streamwise rolls regenerate turbulence in a self-sustaining process (see, e.g. Hamilton et al., 1995; Schoppa and Hussain, 2002). Far from the wall, streamwise coherent structures in the form of long meandering structures are largely responsible for the transport of energy (see, e.g. Kim and Adrian 1999; Guala et al. 2006; Hutchins and Marusic 2007). These observations have inspired the development and exploration of streamwise coherent modeling approaches, that aim to isolate key flow mechanisms, or reduce computational cost while retaining key dynamical features of the flow.

The simplest example of such a model is a two-dimensional three-velocity-component (2D/3C) description of the evolution of a streamwise constant velocity field. The 2D/3C dynamics have been studied in the context of plane Couette (Bobba et al., 2004; Gayme et al., 2010) and Hagen-Poiseuille (Bourguignon and McKeon, 2011) flows. With persistent forcing, the 2D/3C model has been shown to generate streamwise rolls and successfully capture momentum transfer at low Reynolds numbers. However, in the absence of forcing the 2D/3C dynamics are unable to self-sustain turbulence.

The RNL model overcomes the need for external excitation by jointly evolving the streamwise constant mean flow dynamics and a dynamically restricted streamwise varying perturbation field. The resulting coupled dynamics enable self-sustaining turbulence (see, e.g. Farrell et al., 2017). The RNL model falls under a class of quasi-linear (QL) models, which have been widely used in the atmospheric sciences (see, e.g. Farrell and Ioannou 2009; Srinivasan and Young 2012). QL models partition the flow into a large scale (mean flow) and small scale perturbation field and eliminates the nonlinear interactions between the small scales. The large scale is typically a horizontal average (i.e. the zero streamwise and spanwise Fourier components).

The QL paradigm has recently been generalized by employing a spectral filter that includes a range of both streamwise and spanwise length scales in the large scale equation. This generalized quasi-linear (GQL) model has been applied to the study of zonal jets (Marston et al., 2016), the helical magnetorotational instability (Child et al., 2016), and rotating Couette flow (Tobias and Marston, 2017). The RNL model can be obtained as a GQL with wavenumber cut-offs of zero in the streamwise direction and infinity in the spanwise direction.

The resulting restriction of the perturbation field eliminates nonlinear interactions between (streamwise varying) perturbations resulting in a natural order reduction of the streamwise dynamics, where the energy of the large streamwise wavenumbers decay exponentially (Thomas et al., 2015). At $Re_\tau \approx 65$, this unparametrized RNL was shown to accurately predict the mean velocity and reproduce spanwise structures qualitatively similar to those in direct numerical simulation (DNS) data, however the RNL simulations over-predicted the streamwise normal Reynolds stress (Thomas et al., 2014). At higher Reynolds numbers, up to $Re_\tau \approx 950$, RNL simulations have also been found to incorrectly predict the proper log-law behavior (Farrell et al. 2014).

Bretheim et al. (2015) demonstrated how to improve the accuracy of the RNL system in a half-channel

configuration by imposing a different set of streamwise varying wavenumbers. In particular, limiting the streamwise wavenumber support to larger wavenumbers (smaller scales) the accuracy of first- and second-order statistics were shown to improve across a range of Reynolds numbers, $Re_\tau \approx 110,\ 180,\ 260,\ 340$. An analysis across wavenumbers showed that when restricted to a single nonzero streamwise mode, the most accurate statistics predicted by RNL were obtained for wavelengths that asymptotically decreased to $\lambda_x^+ \approx 150$ with increasing Re_τ.

This asymptotic limit of $\lambda_x^+ \approx 150$ also corresponds to the peak of the surrogate dissipation spectra in the outer layer, as plotted by Jiménez (2012) from DNS data at $Re_\tau \approx 2000$. Bretheim et al. (2018) tested this notion in the large eddy simulation (LES) context by developing a RNL-LES model and limiting the streamwise wavenumber support to the range in which the surrogate dissipation peaked in LES. That work showed that a RNL-LES model with such a wavenumber support can correctly predict turbulent statistics at effectively infinite Reynolds numbers.

The current work further explores this dissipation spectra based parametrization of the RNL dynamics by varying the streamwise wavenumber support in a half-channel configuration. First, we compare the streamwise wavenumbers where the surrogate dissipation peaks in DNS to the streamwise wavenumbers identified as being optimal with respect to reproducing log-law behavior in Bretheim et al. (2015), across the Reynolds numbers they considered. We then focus on $Re_\tau \approx 180$ and compare the spectra and energy transport in RNL turbulence supported by large scale streamwise varying structures (the natural support or unparametrized dynamics) to that supported by the "optimal" structures. Our results indicate that the spanwise scales play a role in compensating for simplification of the streamwise varying flow dynamics. The energy transport terms also shift to balance the turbulent kinetic energy budget. We conclude the paper by discussing the implication of these trends and associated directions for future work.

NUMERICAL APPROACH

We consider a half-channel flow configuration, with no-slip and stress-free boundary conditions taken at the bottom ($y = 0$) and top ($y = \delta$) boundaries respectively, and periodic boundary conditions in the streamwise and spanwise directions. A domain size of $[L_x, L_y, L_z]/\delta = [4\pi, 1, 2\pi]$ is used for all simulations.

The RNL dynamics are described by the evolution of a total velocity field $\mathbf{u}_T(x,y,z,t)$ consisting of streamwise (x), wall-normal (y), and spanwise (z) velocity components, respectively denoted (u_T, v_T, w_T). Taking angle brackets to denote streamwise averaging (represented in Fourier space as $k_x = 0$), the total velocity is decomposed into a streamwise mean component, $\mathbf{U}(y,z,t) = \langle \mathbf{u}_T \rangle$, and perturbations about that mean $\mathbf{u}(x,y,z,t) = \mathbf{u}_T - \mathbf{U}$. The RNL dynamics are governed by continuity of the total velocity, $\nabla \cdot \mathbf{u}_T = 0$, and the momentum equations,

$$\partial_t \mathbf{U} + \mathbf{U}\cdot\nabla\mathbf{U} + \nabla P/\rho - \nu\nabla^2\mathbf{U} = -\langle \mathbf{u}\cdot\nabla\mathbf{u}\rangle \qquad \text{(1a)}$$

$$\partial_t \mathbf{u} + \mathbf{U}\cdot\nabla\mathbf{u} + \mathbf{u}\cdot\nabla\mathbf{U} + \nabla p/\rho - \nu\nabla^2\mathbf{u} = 0\,. \qquad \text{(1b)}$$

Had the Navier-Stokes equations been decomposed in this manner, the resulting equations would include the nonlinear term, $\langle \mathbf{u}\cdot\nabla\mathbf{u}\rangle - \mathbf{u}\cdot\nabla\mathbf{u}$, on the right hand side of equation (1b). Omitting this term restricts the nonlinear interactions of the perturbations to interactions with the mean flow and those that result in streamwise constant flow i.e. those represented in in Fourier space as $k_{x,m} + k_{x,n} = 0$. Here the dimensional streamwise wavenumber is defined as $k_{x,n} = 2\pi n/L_x$. The corresponding streamwise wavelength is defined as $\lambda_x = 2\pi/k_x$.

We simulate equation (1) using the open source pseudo-spectral code LESGO (https://lesgo.me.jhu.edu). This code employs a second-order central finite difference scheme in the wall-normal direction and spectral discretization in the homogeneous directions, where the 3/2 rule is used for dealiasing. To advance the simulations in time, the second-order Adams-Bashforth method is used.

We run DNS at $Re_\tau \approx 110,\ 180,\ 260,\ 340$, where the friction Reynolds number is defined as $Re_\tau = u_\tau\delta/\nu$, with friction velocity u_τ. RNL simulations are performed at $Re_\tau \approx 180$ and compared to DNS. DNS and RNL simulations are run with the same wall-normal and spanwise grid resolutions. The wall-normal grid is stretched using a hyperbolic tangent function, five grid points exist below $y^+ = 5$ and consecutive grid points are stretched with the ratio satisfying $\Delta y_{n+1}/\Delta y_n < 1.03$. The spanwise grid spacing is $\Delta z^+ \approx 8$. The superscript $+$ indicates scaling by viscous length scale $\delta_\nu = \nu/u_\tau$.

The streamwise grid resolution of the DNS is $\Delta x^+ \approx 8$ and the nonlinear term is computed in the physical space, requiring transformations back and forth to compute derivatives in Fourier space. When simulating the RNL system, we take advantage of the simplified streamwise dynamics and compute the nonlinearity in (k_x, y, z, t) space, see Bretheim et al. (2018) for more details.

Eliminating the need for these transforms in the streamwise direction saves computational time and resources. With the same number of processors on the same hardware, the RNL simulations performed in this work showed a wall-time speedup of 19.1× compared to DNS. In the following section results from DNS and RNL simulations are presented.

RESULTS

We begin by showing that the streamwise wavelengths associated with reproducing log-law behavior in RNL, found empirically by Bretheim et al. (2015), coincide with the peak of the surrogate dissipation spectra in the outer layer at low to moderate Reynolds numbers. Bretheim et al. (2015) computed these streamwise wavelengths by running a series of RNL simulations where they varied the single nonzero streamwise wavenumber ($k_x \neq 0$ Fourier component) supporting the dynamics. At a fixed Reynolds number, they then reported the simulation which most accurately predicted the skin-friction coefficient. These associated streamwise wavelengths for each Re_τ that they simulated are presented in the top left panel of figure 1.

The remaining panels of figure 1 show the corresponding pre-multiplied streamwise surrogate dissipation spectra predicted by DNS at various Reynolds numbers, with a dashed line indicating the values from Bretheim et al. (2015). The surrogate dissipation spectra is computed as the time-fluctuating vorticity (Jiménez 2012) and differs from the true dissipation by a cross-term of velocity gradients that is identically zero in homogeneous isotropic turbulence, and is relatively small in channel flow.

Figure 1 demonstrates good agreement between the

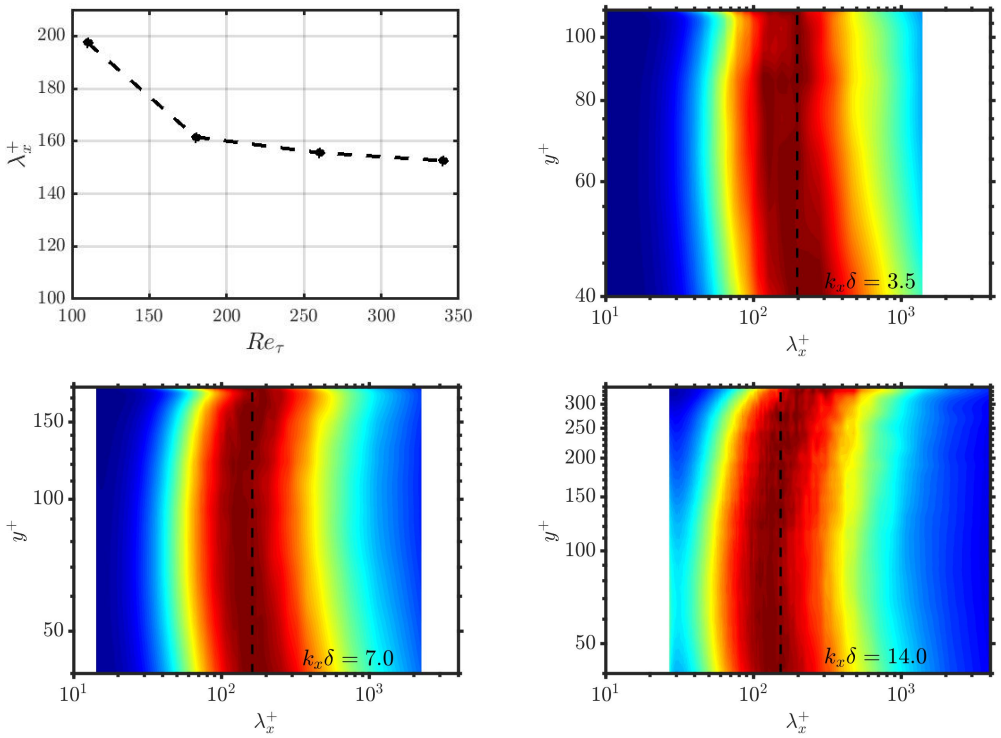

Figure 1: The optimal streamwise wavelengths found empirically in Bretheim et al. (2015) (top left) is shown to coincide with the peak of the pre-multiplied streamwise surrogate dissipation spectra ($\nu k_x(E_{\omega_x\omega_x}+E_{\omega_y\omega_y}+E_{\omega_z\omega_z})$) at Re_τ: 110 (top right), 180 (bottom left), and 340 (bottom right). The spectra is locally normalized by its maximum value at each y^+, with color scale from 0 (blue) to 1 (red). The vertical black dashed lines in the spectra correspond to the streamwise wavelength at that Re_τ given in Bretheim et al. (2015) shown in the top left panel.

streamwise wavelengths predicted by Bretheim et al. (2015) and the streamwise wavelengths where the surrogate dissipation peaks in the outer layer. It should be mentioned that near the wall, the surrogate dissipation peaks at streamwise wavelengths larger than those in the outer layer. Therefore the streamwise scales that reproduce the correct momentum transfer in the RNL system are associated with the peak surrogate dissipation in the outer layer, even though it is near the wall where majority of the energy is dissipated.

We now focus on RNL turbulence at $Re_\tau \approx 180$ and further examine energy transport in the RNL dynamics. More specifically, we characterize how the spectra and energy transport are affected when we move the streamwise wavenumber support from the low wavenumbers associated with the unparameterized RNL dynamics to the more dissipative streamwise scales.

Two RNL simulations at $Re_\tau \approx 180$ are performed. The first with a streamwise wavenumber support consisting of the modes that comprise the unparameterized RNL dynamics, labelled R-1. The second RNL simulation, labelled R-2, includes the modes associated with the peak of the surrogate dissipation structure (i.e. known to lead to a mean flow with the correct log-law). Both wavenumber supports include the streamwise mean component ($k_x = 0$) as well as three consecutive non-zero streamwise wavenumbers, $k_x\delta = 0.5,\ 1.0,\ 1.5$ in simulation R-1 and $k_x\delta = 6.0,\ 6.5,\ 7.0$ in simulation R-2.

First- and second-order statistics obtained through simulations of cases R-1 and R-2 are compared in figure 2, where time-averaged quantities are denoted by a over-bar and fluctuations with respect to this average are denoted by a prime. The mean velocity of the R-1 case agrees well with the law of the wall in the viscous sub-layer, however as in previous studies (Bretheim et al., 2015; Farrell et al., 2016;) it predicts a higher velocity than the log-law. As expected the Reynolds shear stress follows a similar trend reaching a higher minimum value than that of the DNS further from the wall. Also, as seen in previous studies, the peak in the streamwise and wall-normal Reynolds stresses occur further from the wall when compared to the DNS data. The R-1 simulation also over predicts the streamwise and under predicts the cross stream Reynolds stresses (only the wall-normal component is shown) throughout the channel domain.

Figure 2 shows that the accuracy of the first- and second-order statistics of the R-2 case improve compared to the R-1 case. All second-order statistics from the R-2 case peak at the same distance from the wall as the DNS. The magnitudes of the Reynolds stresses are also closer to those of the DNS compared to the R-1 case, however the streamwise component is still higher and the wall-normal component is still lower. These results demonstrate supporting RNL turbulence with wavenumbers corresponding to the peak of the surrogate dissipation spectra improves the accuracy of the model.

We next examine how the change in streamwise wavenumber support affects the spanwise energy spectra of RNL turbulence. The streamwise and wall-normal component of the pre-multiplied spanwise energy spectra is plotted in figure 3. This figure shows that restricting the streamwise dynamics to larger streamwise scales, as in R-1, results in the spectra peaking at larger spanwise scales com-

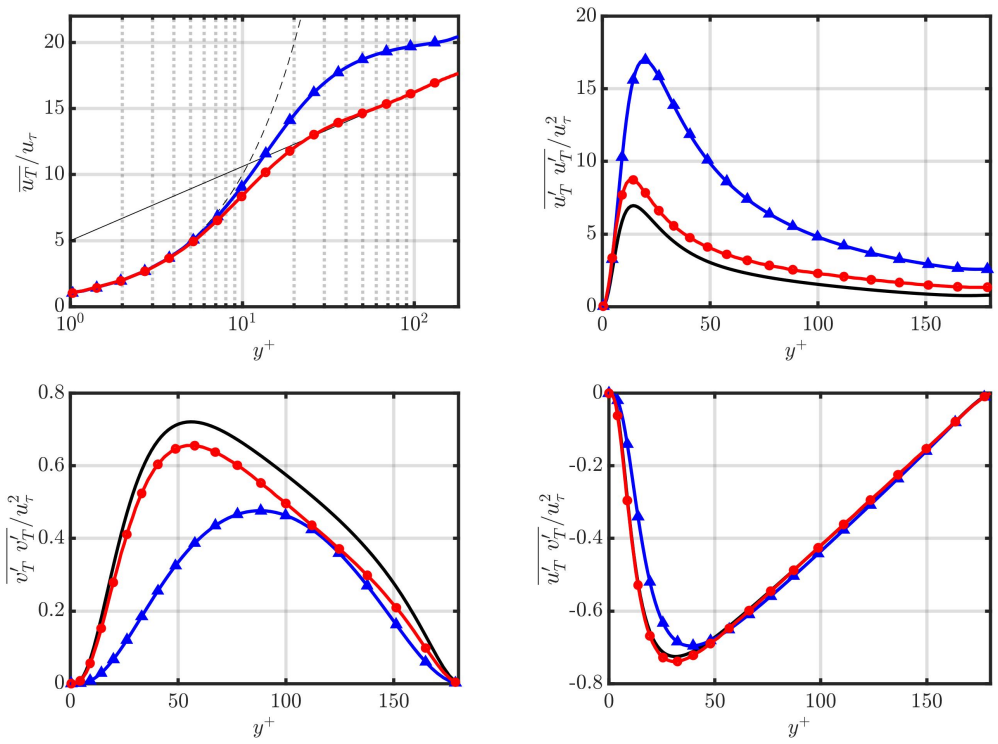

Figure 2: RNL with large streamwise wavenumbers (R-1, blue triangles) shown to incorrectly predict mean velocity (top left) and Reynolds stress (top right, bottom left, bottom right) profiles. The accuracy of these statistics is improved for RNL dynamics with a streamwise wavenumber support associated with the outer layer surrogate dissipation peak (R-2, red circles). Reynolds stress profiles from DNS shown as thick black lines, $\overline{u_T}/u_\tau = y^+$ (thin dashed black) and $\overline{u_T}/u_\tau = (1/0.41)\log(y^+) + 5.0$ (thin solid black) shown with mean velocity profiles. Markers are subsampled for clairty and do not represent grid resolution.

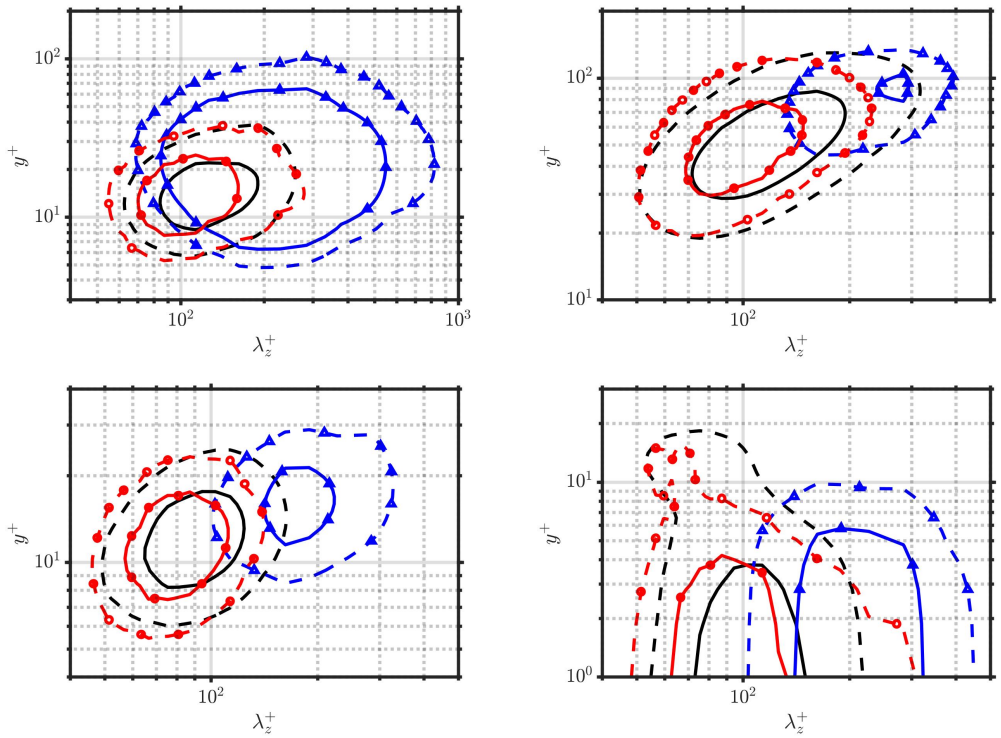

Figure 3: Pre-multiplied spanwise energy spectra, $k_z E_{uu}$ (top left), $k_z E_{vv}$ (top right), production rate spectra $k_z \tilde{P}$ (bottom left), and surrogate dissipation spectra $\nu k_z (E_{\omega_x\omega_x} + E_{\omega_y\omega_y} + E_{\omega_z\omega_z})$ (bottom right) for case R-1 (blue triangles) peak at large spanwise scales. The spectra for case R-2 (red circles) is closer to DNS (black), yet peak at even smaller spanwise scales to compensate for the simplified streamwise dynamics. Solid lines are 0.80 times the maximum from DNS, dashed lines are 0.50 times the maximum.

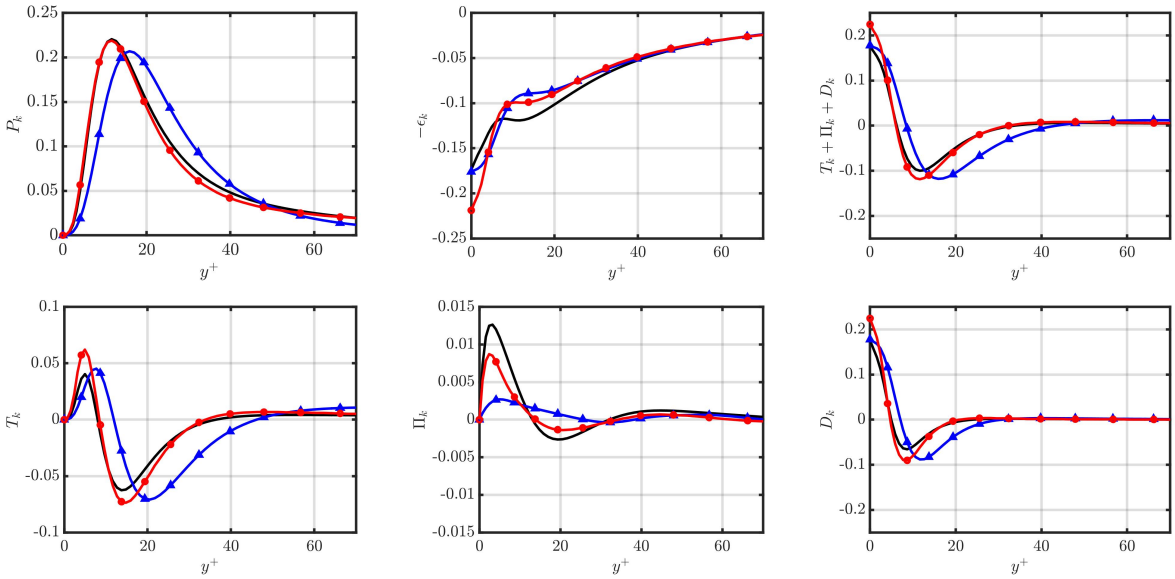

Figure 4: Terms of the turbulent kinetic energy budget for R-1 (blue triangles), R-2 (red circles), and DNS (black). The top figures include production rate (left), pseudo-dissipation rate (middle) and summation of transport terms (right). The bottom figures provide the individual transport terms: turbulent transport (left), pressure transport (middle), and viscous transport (right).

pared to DNS. The restriction of the dynamics to the largest streamwise structures also leads to the streamwise component of the pre-multiplied spanwise spectra spanning a broader range of scales, and the wall-normal component becoming more concentrated.

Supporting the RNL dynamics with the smaller scale structures, which leads to more accurate flow statistics (as in case R-2), results in a shift of the peaks of the energy spectra to smaller spanwise scales. The overall shape and peak location of the spectra becomes more accurate (i.e. closer to DNS) however the peak occurs at lower spanwise scales. This shift can be interpreted as a compensation for the simplified streamwise dynamics comprised of less small scale activity in the streamwise direction. The additional dissipation by the spanwise structures enable the properly parameterized RNL dynamics (case R-2) to develop the correct log-law behavior.

The production and surrogate dissipation of the spanwise energy spectra is provided in figure 3. The production rate spectra, computed as a product of the pre-multiplied velocity cospectra, $k_z E_{uv}$, and the mean velocity gradient, shows a similar trend for the R-1 and R-2 cases to that observed in the energy spectra. The surrogate dissipation rate of the spanwise energy spectra, which peaks at the wall, extends further from the wall for the R-1 case than the DNS and R-2 case. These quantities also show the shifting of the peak values towards smaller spanwise scales supporting the notion that the system is compensating for the simplified streamwise dynamics by altering the spanwise structures.

We further examine energy transport in the RNL dynamics by plotting the production, transport, and pseudo-dissipation rates of the turbulent kinetic energy in figure 4. The y^+ axis of these figures is focused in the near wall region since significant changes of the terms in the budget are not observed in the outer layer. The production rate and summation of all transport terms for the R-1 case reach minimum and maximum values further from the wall compared to DNS. This agrees with trends observed in figures 2 and 3. At $y^+ \approx 17$, the production and pseudo-dissipation rates for case R-1 have smaller magnitudes compared to those seen in the DNS. The turbulent kinetic energy budget is then balanced by an increase in the magnitude of the the total transport in that location. The bottom panels of figure 4 plots each of the transport terms individually. These figures indicate that this increase in magnitude is due to turbulent and viscous transport, rather than pressure transport.

Again selecting the RNL support based on the peak of the surrogate dissipation spectra (case R-2) results in the production rate and transport terms having peak magnitudes in similar locations to those of the DNS, which supports the observations of figures 2 and 3. In the viscous sublayer and buffer layer, the production rate predicted by the R-2 case agrees well with DNS, however the pseudo-dissipation is higher in the viscous sublayer and lower in the buffer layer. The transport terms then balance this discrepancy with higher magnitudes in those regions. Similar to the R-1 case, higher turbulent and viscous transport are observed in the R-2 case, however the R-2 case also reaches higher pressure transport values compared to the R-1 case.

CONCLUSIONS

The RNL wavenumber support identified as reproducing the correct momentum transfer in Bretheim et al. (2015) has been related to the peak of the surrogate dissipation spectra across low to moderate Reynolds numbers. At higher Reynolds numbers this value asymptotes to $\lambda_x^+ \approx 150$, implying that RNL could be used as a predictive reduced-order model.

The streamwise wavenumber support leading to improved accuracy of the RNL statistical features introduces smaller streamwise scales, which leads to more accurate energy transfer. However, the peak in the energy spectra corresponds to smaller spanwise scales suggesting that the RNL dynamics use the spanwise components to compensate for the reduction in nonlinear interactions at small streamwise

scales. Near the wall the properly parameterized RNL is shown to accurately predict the production rate, however pseudo-dissipation is higher in the viscous sublayer and lower in the buffer layer compared to DNS. The turbulent kinetic energy budget is then balanced by corresponding shifts in the turbulent and viscous transport rates.

These trends suggest that the statistical features of turbulence are very robust, i.e. the flow adjusts the energy transport to maintain the turbulent state. A deeper understanding of this behavior is an interesting direction for future work, particularly in relation to flow control that aims to alter the turbulent dynamics.

ACKNOWLEDGEMENTS

We thank Xiaowei Zhu for helpful discussions and implementing the stretched grid code. We gratefully acknowledge support from the National Science Foundation (CBET 1652244) and the Office of Naval Research (N000141712649). We also acknowledge the computational resources used to conduct these simulations at the Maryland Advanced Research Computing Center (MARCC).

REFERENCES

Bobba, K., Doyle, J. & Gharib, M. 2004 A Reynolds number independent model for turbulence in Couette flow. *IUTAM Symposium on Reynolds number scaling in turbulent flow* **74**, 145–149.

Bourguignon, J.-L. & McKeon, B. J. 2011 A streamwise-constant model of turbulent pipe flow. *Phys. Fluids* **23**, 095111.

Bretheim, J., Meneveau, C. & Gayme, D. F. 2015 Standard logarithmic mean velocity distribution in a band-limited restricted nonlinear model of turbulent flow in a half-channel. *Phys. Fluids* **27**, 011702.

Bretheim, J. U., Meneveau, C. & Gayme, D. F. 2018 A restricted nonlinear large eddy simulation model for high Reynolds number flows. *J. Turbul.* **19:2**, 141–166.

Child, A., Hollerbach, R., Marston, B. & Tobias, S. 2016 Generalised quasilinear approximation of the helical magnetorotational instability. *J. Plasma Phys.* **82**, 1–18.

Farrell, B. F., Gayme, D. F. & Ioannou, P. J. 2017 A statistical state dynamics approach to wall turbulence. *Phil. Trans. R. Soc. A* **375**, 20160081.

Farrell, B. F. & Ioannou, P. J. 2008 A theory of baroclinic turbulence. *J. Atmos. Sci.* **66**, 2444–2454.

Farrell, B. F., Ioannou, P. J., Jiménez, J., Constantinou, N. C., Lozano-Durán, A. & Nikolaidis, M.-A. 2016 A statistical state dynamics-based study of the structure and mechanism of large-scale motions in plane Poiseuille flow. *J. Fluid Mech.* **809**, 290–315.

Gayme, D. F., McKeon, B. J., Papachristodoulou, A., Bamieh, B. & Doyle, J. C. 2010 A streamwise constant model of turbulence in plane Couette flow. *J. Fluid Mech.* **665**, 99–119.

Guala, M., Hommema, S. E. & Adrian, R. J. 2006 Large-scale and very-large-scale motions in turbulent pipe flow. *J. Fluid Mech.* **554**, 521–542.

Hamilton, J., Kim, J. & Waleffe, F. 1995 Regeneration mechanisms of near-wall turbulence structures. *J. Fluid Mech.* **287**, 317–348.

Hutchins, N. & Marusic, I. 2007 Large-scale influences in near-wall turbulence. *Phil. Trans. R. Soc. Lond.* **365**, 647–664.

Jiménez, J. 2012 Cascades in wall-bounded turbulence. *Ann. Rev. Fluid Mech.* **44**, 27–45.

Kim, K. C. & Adrian, R. J. 1999 Very large-scale motion in the outer layer. *Phys. Fluids* **11**, 417–422.

Marston, J. B., Chini, G. P. & Tobias, S. M. 2016 Generalized quasilinear approximation: Application to zonal jets. *Phys. Rev. Lett.* **116**.

Schoppa, W. & Hussain, F. 2002 Coherent structure generation in near-wall turbulence. *J. Fluid Mech.* **453**, 57–108.

Smits, A. J., McKeon, B. J. & Marusic, I. 2011 High-Reynolds number wall turbulence. *Annu. Rev. Fluid Mech.* **43**, 353–375.

Srinivasan, K. & Young, W. R. 2012 Zonostrophic instability. *J. Atmos. Sci.* **69**, 2229–2253.

Thomas, V. L., Farrell, B., Ioannou, P. J. & Gayme, D. F. 2015 A minimal model of self-sustaining turbulence. *Phys. Fluids* **27**, 105104.

Thomas, V. L., Lieu, B. K., Jovanovic, M. R., Farrell, B., Ioannou, P. J. & Gayme, D. F. 2014 Self-sustaining turbulence in a restricted nonlinear model of plane Couette flow. *Phys. Fluids* **26**, 105112.

Tobias, S. M. & Marston, J. B. 2017 Three-dimensional rotating Couette flow via the generalised quasilinear approximation. *J. Fluid Mech.* **810**, 412–428.